



OPEN

DATA DESCRIPTOR

RNA-seq profiling of white and brown adipocyte differentiation treated with epigallocatechin gallate

Pengpeng Zhang^{1,2,3}, Wei Wu^{1,3}, Chunyu Du¹, Xiang Ji¹, Yaling Wang¹, Qiu Han¹, Hiaxia Xu¹, Cencen Li¹✉ & Yongjie Xu^{1,2}✉

Due to serious adverse effects, many of the approved anti-obesity medicines have been withdrawn, and the selection of safer natural ingredients is of great interest. Epigallocatechin gallate (EGCG) is one of the major green tea catechins, and has been demonstrated to possess an anti-obesity function by regulating both white and brown adipose tissue activity. However, there are currently no publicly available studies describing the effects of EGCG on the two distinct adipose tissue transcriptomes. The stromal vascular fraction (SVF) cell derived from adipose tissue is a classic cell model for studying adipogenesis and fat accumulation. In the current study, primary WAT and BAT SVF cells were isolated and induced to adipogenic differentiation in the presence or absence of EGCG. RNA-seq was used to determine genes regulated by EGCG and identify the key differences between the two functionally distinct adipose tissues. Taken together, we provide detailed stage- and tissue-specific gene expression profiles affected by EGCG. These data will be valuable for obesity-related clinical/basic research.

Background & Summary

Obesity is defined as abnormally excessive body fat accumulation. It has been accepted as one of the global health issues because it is highly associated with many diseases such as diabetes, dyslipidemia, and cardiovascular diseases¹, which are harmful to health and lead to significant economic and social burdens in many countries worldwide.

The main feature of obesity is enlarged adipose tissue, which is dependent on hyperplasia (formation of new adipocytes from precursor cells) and hypertrophy of pre-existing adipocytes². Animal adipose tissue mainly includes white adipose tissue (WAT) and brown adipose tissue (BAT), which could be distinguished from cell structures and functional roles. Many large lipid droplets accumulate in WAT, while only a few small lipid droplets can be identified in BAT. Whereas WAT stores energy as triglycerides, BAT generates heat through fatty acid metabolism³. Therefore, strategies that regulate WAT adipocyte size, number, or stimulation of BAT are considered a possible therapeutic approach for combating obesity⁴.

Medical approaches to the prevention and treatment of obesity include anti-obesity drugs and surgery. Because surgery is limited to severely obese individuals, anti-obesity drugs are a promising solution to obesity. However, many adverse drug reactions or side effects have raised public concern⁵. Hence, the selection of natural products with high anti-obesity efficacy, safety, and long-term effects is receiving more attention.

Recently, the anti-obesity effects of green tea have been greatly investigated. Green tea catechins are the predominant form of flavor, which can be extracted from green tea. It has been reported that green tea catechins, especially epigallocatechin gallate (EGCG) could decrease fat accumulation⁶. Evidence from *in vitro* and *in vivo* studies indicates that EGCG plays role in various nutritional and pharmacological functions, including anti-inflammatory⁷, antioxidative⁸, antiangiogenesis⁹, and cardiovascular protection effects¹⁰. Recent studies also demonstrated that EGCG regulates both WAT and BAT activity. It could not only reduce white adipose tissue mass by inhibiting the synthesis of *de novo* fatty acids and increasing lipolysis¹¹, but also increase

¹Department of Biotechnology, College of Life Sciences, Xinyang Normal University, Xinyang, China. ²Institute for Conservation and Utilization of Agro-Bioresources in Dabie Mountains, Xinyang Normal University, Xinyang, China.

³These authors contributed equally: Pengpeng Zhang, Wei Wu. ✉e-mail: licencen2009@126.com; yongjx81@126.com

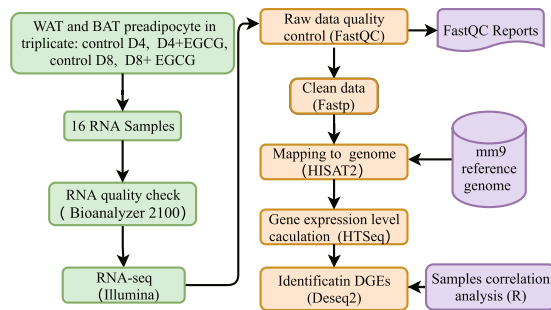


Fig. 1 The workflow of data collection and technical analysis for this study.

| Subject | Source | Treatment | Sample Name | Protocol 1 | Protocol 2 | GEO Accession |
|-------------------------|-----------------------|-----------|-------------|----------------|------------|---------------|
| mouse WAT replication 1 | differentiation day 4 | Control | mW41 | RNA extraction | RNA-seq | GSE173710 |
| mouse WAT replication 2 | differentiation day 4 | Control | mW42 | RNA extraction | RNA-seq | GSE173710 |
| mouse WAT replication 3 | differentiation day 4 | Control | mW43 | RNA extraction | RNA-seq | GSE173710 |
| mouse WAT replication 1 | differentiation day 4 | Control | mW81 | RNA extraction | RNA-seq | GSE173710 |
| mouse WAT replication 2 | differentiation day 4 | Control | mW82 | RNA extraction | RNA-seq | GSE173710 |
| mouse WAT replication 3 | differentiation day 4 | Control | mW83 | RNA extraction | RNA-seq | GSE173710 |
| mouse WAT replication 1 | differentiation day 8 | EGCG | mWE41 | RNA extraction | RNA-seq | GSE173710 |
| mouse WAT replication 2 | differentiation day 8 | EGCG | mWE42 | RNA extraction | RNA-seq | GSE173710 |
| mouse WAT replication 3 | differentiation day 8 | EGCG | mWE43 | RNA extraction | RNA-seq | GSE173710 |
| mouse WAT replication 1 | differentiation day 8 | EGCG | mWE81 | RNA extraction | RNA-seq | GSE173710 |
| mouse WAT replication 2 | differentiation day 8 | EGCG | mWE82 | RNA extraction | RNA-seq | GSE173710 |
| mouse WAT replication 3 | differentiation day 8 | EGCG | mWE83 | RNA extraction | RNA-seq | GSE173710 |
| mouse BAT replication 1 | differentiation day 4 | Control | mB41 | RNA extraction | RNA-seq | GSE173710 |
| mouse BAT replication 2 | differentiation day 4 | Control | mB42 | RNA extraction | RNA-seq | GSE173710 |
| mouse BAT replication 3 | differentiation day 4 | Control | mB43 | RNA extraction | RNA-seq | GSE173710 |
| mouse BAT replication 1 | differentiation day 4 | Control | mB81 | RNA extraction | RNA-seq | GSE173710 |
| mouse BAT replication 2 | differentiation day 4 | Control | mB82 | RNA extraction | RNA-seq | GSE173710 |
| mouse BAT replication 3 | differentiation day 4 | Control | mB83 | RNA extraction | RNA-seq | GSE173710 |
| mouse BAT replication 1 | differentiation day 8 | EGCG | mBE41 | RNA extraction | RNA-seq | GSE173710 |
| mouse BAT replication 2 | differentiation day 8 | EGCG | mBE42 | RNA extraction | RNA-seq | GSE173710 |
| mouse BAT replication 3 | differentiation day 8 | EGCG | mBE43 | RNA extraction | RNA-seq | GSE173710 |
| mouse BAT replication 1 | differentiation day 8 | EGCG | mBE81 | RNA extraction | RNA-seq | GSE173710 |
| mouse BAT replication 2 | differentiation day 8 | EGCG | mBE82 | RNA extraction | RNA-seq | GSE173710 |
| mouse BAT replication 3 | differentiation day 8 | EGCG | mBE83 | RNA extraction | RNA-seq | GSE173710 |

Table 1. RNA-seq samples information.

thermogenesis and mitochondrial biogenesis in brown adipose tissues¹². However, a systemic comparison of transcriptomes that are affected by EGCG in both WAT and BAT is lacking, which is of great interest to the field.

To address this question, primary WAT and BAT preadipocytes were isolated and induced adipogenic differentiation in the presence or absence of EGCG. Samples were collected on Day 4 and Day 8 post differentiation, which represented the early and mature stages of adipogenesis, respectively. Then, we performed Illumina RNA-seq and bioinformatics analysis of the mRNA profile (Fig. 1). This comprehensive dataset will provide the stage- and tissue-specific effects of EGCG on adipogenesis and fat storage. The dataset might be a very useful resource to researchers for the development of therapies to treat obesity and other metabolic diseases.

Methods

Cell culture. All procedures involving mice were approved by the Xinyang Normal University Animal Care and Use Committee. Primary WAT and BAT stromal vascular fraction (SVF) cells were isolated as previously described^{13,14}. Briefly, inguinal WAT and interscapular BAT were obtained from 6-week-old mice on a C57BL/6J background. Fat pads were cut into small pieces and incubated with collagenase digestion solution (1.5 mg ml⁻¹, #SCR103, Sigma-Aldrich). WAT was incubated for 30 min and BAT was incubated for 50 min. Then, an equal volume of growth medium (DMEM containing 20% FBS) was added to terminate digestion. To remove tissue debris, the digestion was filtered through 100- μ m and 70- μ m cell trainers. Next, it was centrifuged at 450 g for 8 min. Then, the SVF cells pellet was resuspended and cultured in growth medium, at 37°C with 5% CO₂. When the cells reached 90% confluence, the growth medium was changed to DMEM containing 10% FBS, and the cells

| Sample Name | Sequencing Strategy | Raw reads number | Clean reads number | Q20 | Q30 | Mapping rate (%) |
|-------------|---------------------|------------------|--------------------|-------|-------|------------------|
| mW41 | PE150 | 63353952 | 62659858 | 98.05 | 94.45 | 91.20 |
| mW42 | PE150 | 53454310 | 52794832 | 98.04 | 94.44 | 91.38 |
| mW43 | PE150 | 21568205 | 20498381 | 98.06 | 94.71 | 88.61 |
| mW81 | PE150 | 56009120 | 55212996 | 98.00 | 94.31 | 90.98 |
| mW82 | PE150 | 59735598 | 58768178 | 98.04 | 94.42 | 91.40 |
| mW83 | PE150 | 21857011 | 20971455 | 97.97 | 94.44 | 88.46 |
| mWE41 | PE150 | 61953094 | 60984426 | 97.81 | 93.88 | 91.57 |
| mWE42 | PE150 | 49808446 | 49100258 | 98.12 | 94.63 | 91.49 |
| mWE43 | PE150 | 31188130 | 29905593 | 97.97 | 94.45 | 88.54 |
| mWE81 | PE150 | 64305198 | 63472412 | 97.93 | 94.13 | 91.92 |
| mWE82 | PE150 | 49264074 | 48649180 | 98.01 | 94.35 | 91.92 |
| mWE83 | PE150 | 21438213 | 20127271 | 97.99 | 94.56 | 88.99 |
| mB41 | PE150 | 50653710 | 49932582 | 98.03 | 94.37 | 91.83 |
| mB42 | PE150 | 56322254 | 55589762 | 98.08 | 94.51 | 91.81 |
| mB43 | PE150 | 23036272 | 21796117 | 97.98 | 94.52 | 87.57 |
| mB81 | PE150 | 55074040 | 54072312 | 97.99 | 94.29 | 92.04 |
| mB82 | PE150 | 61684398 | 60751782 | 97.93 | 94.13 | 91.92 |
| mB83 | PE150 | 23510964 | 22462259 | 98.03 | 94.58 | 88.10 |
| mBE41 | PE150 | 58047352 | 57059452 | 98.16 | 94.68 | 92.07 |
| mBE42 | PE150 | 48561368 | 47888428 | 98.08 | 94.51 | 91.97 |
| mBE43 | PE150 | 24374910 | 23127966 | 98.03 | 94.61 | 88.80 |
| mBE81 | PE150 | 57668480 | 56867060 | 98.07 | 94.51 | 92.47 |
| mBE82 | PE150 | 64849394 | 63939362 | 98.01 | 94.37 | 92.47 |
| mBE83 | PE150 | 22612540 | 21115135 | 97.99 | 94.56 | 89.24 |

Table 2. RNA-seq reads information.

were induced to adipogenic differentiation by supplementation with a cocktail containing 2.85 mM recombinant human insulin (#I8830, Solarbio), 0.3 mM dexamethasone (#D8040, Solarbio), and 0.63 mM 3-isobutyl-methylxanthine (#I7018, Sigma-Aldrich). After four days, the cocktail was changed to 200 nM insulin, and 10 nM T3 (#T6397, Sigma-Aldrich) to induce mature adipocytes. EGCG (5 μ M) or DMSO control (1:1000) was added to the induction medium and differentiation medium from Day 4 to 8 of adipogenesis. The medium was changed every 2 days. To examine the lipid droplets, oil red O staining was performed. Briefly, the mature adipocytes were washed twice with PBS. Then, the cells were fixed with 10% formaldehyde for 5 min. Next, the cells were stained with Oil red O staining solutions (#G1262, Solarbio) for 30 min. After staining, the images were captured with an Axio Observer 3 Zeiss microscope (Carl Zeiss, Germany).

RNA reparation. TRIzol (#15596026, Thermo Fisher Scientific) was used to collect RNA. RNA concentration was measured using a Qubit[®] RNA Assay Kit in a Qubit[®] 2.0 Fluorometer (Life Technologies, USA). A Bioanalyzer 2100 system (Agilent Technologies, USA) was used to examine RNA integrity.

Real-time PCR analysis. Real-time PCR was performed as previously described¹⁵. Briefly, Reverse Transcription Kit (#RR037A, Takara) was used to synthesize cDNA. Real-time PCR was performed on a CFX96 Real-Time System (Bio-Rad Laboratories, Singapore) according to the manufacturer's instructions. 18S was used as housekeeping genes. The ($2^{-\Delta\Delta C_t}$) method was used to calculate the gene expression levels.

RNA-Seq library construction, RNA-sequencing, and bioinformatics analysis. The sequencing library was built using the NEBNext[®] UltraTM RNA Library Prep Kit for Illumina[®] (#E7530L, NEB), and 3 μ g RNA for each sample was used. Clustering of the index-coded samples was performed on a cBot Cluster Generation System using TruSeq PE Cluster Kit v3-cBot-HS (#PE-401-3001, Illumina) according to the manufacturer's instructions. Sequencing was carried out on an Illumina HiSeq 4,000 platform. 150-bp paired-end reads were generated.

Bioinformatics analyses. Quality control of sequences was examined with FastQC (version 0.11.9)¹⁶. Clean data were obtained using Fastp (version 0.20.1)¹⁷ to remove low-quality reads, read adapters, and reads containing poly-N. Then, the clean data were subjected to mapping with the *Mus musculus* mm9 genome reference by HISAT2 (version 2.2.0)¹⁸. The average input read count was 44.91 million per sample (range 20.12 million to 63.9 million), and the average percentage of uniquely aligned reads was 90.70% (range 87.57% to 92.5%). The read counts for each gene were calculated by HTSeq (version 0.11)¹⁹. The third biological replication was sequenced at different batches as the other biological replications. The expression levels were corrected for batch effects using the Combat_Seq function from the SVA R package (version 3.42.0)²⁰. Principal component analysis (PCA) was generated with FactoMineR²¹ to assess variance between sample groups and sample replicates. Differential gene

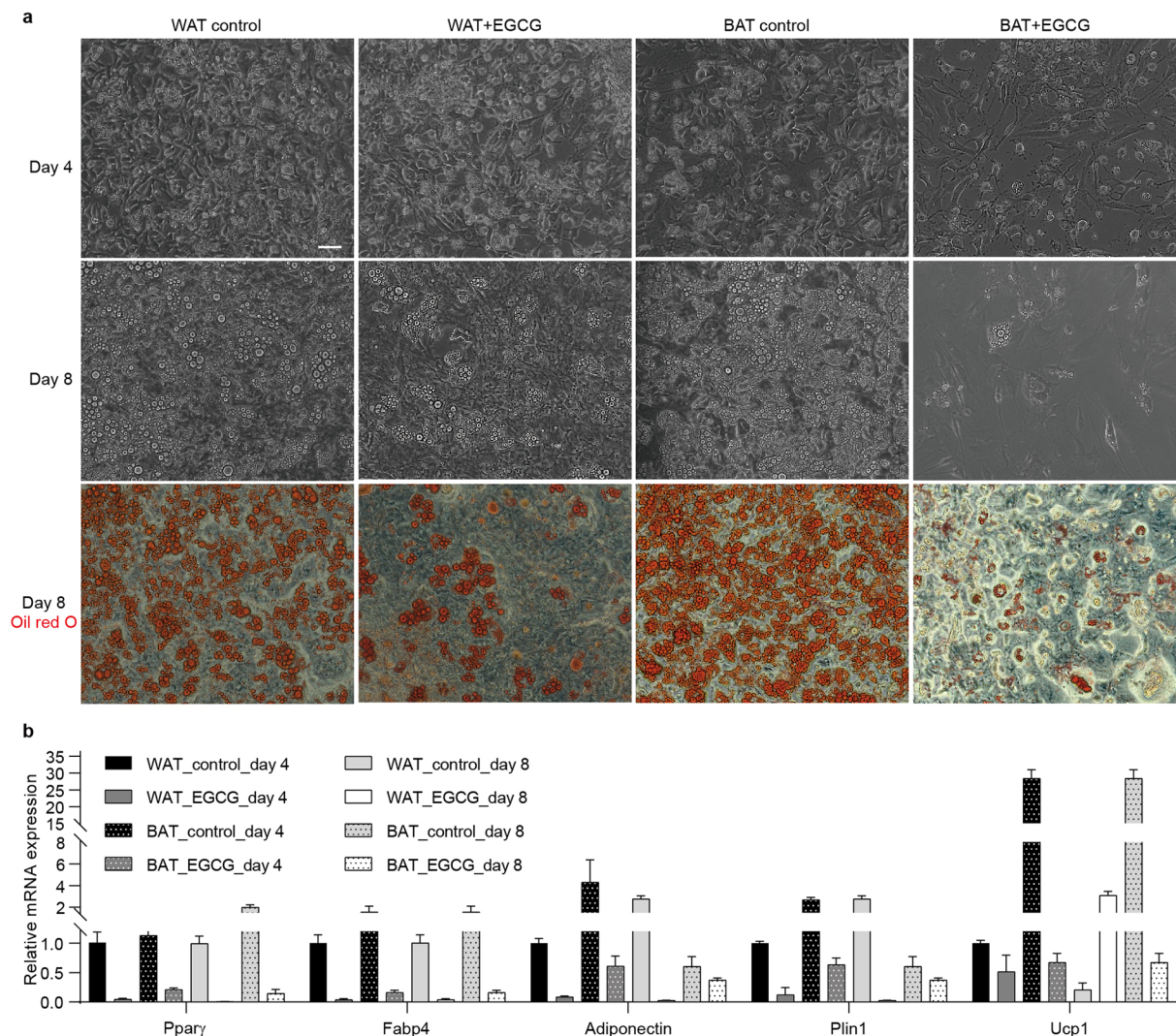


Fig. 2 Differentiation of WAT and BAT SVF cells. **(a)** Representative pictures of the cells at Day 4 and Day 8 post differentiation. Oil red O staining was performed to visualize lipid droplets at Day 8 post differentiation. Scale bar = 20 μ m. **(b)** Relative expression of the selected white and brown adipocyte marker genes ($n = 3$). Mean and standard deviations are shown.

expression was identified by DESeq2 (version 1.10.1). A heatmap was generated with pheatmap (version 1.0.12)²² to show the differentially expressed genes between the control and EGCG-treated group. The R package ggplot2 (version 3.3.4)²³ was used to generate volcano plots and compare the gene expression levels between the control and EGCG-treated groups.

Data Records

The RNA-Seq data were deposited in the NCBI Sequence Read Archive (SRA) under the accession number SRP318155²⁴. The metadata records regarding the sample's information and RNA-seq read statistics are provided in Tables 1 and 2, respectively.

Technical Validation

Quality control of cell differentiation. The quality of WAT and BAT SVF adipogenic differentiation was examined at Day 4 and Day 8 post differentiation. As shown in Fig. 2a, the cells underwent a morphology change, from spindle to round and small droplets began to accumulate at Day 4 in the control groups. Furthermore, many more large droplets accumulated at Day 8 post differentiation. Oil red O staining showed that both WAT and BAT SVF cells differentiated well at Day 8. Compared to the control groups, the SVF cells treated with EGCG showed fewer lipid droplets, which indicated that EGCG inhibits SVF cells adipogenic differentiation. Consistent with these findings, real-time PCR analysis showed that adipose marker genes (*Ppar γ* , *Fabp4*, *Adiponectin*, and *Plin1*) were expressed at much higher levels in the control groups than in the EGCG treated groups. In addition, the BAT SVF cells in the control groups expressed approximately 30 times more *Ucp1* (BAT marker gene) than the WAT

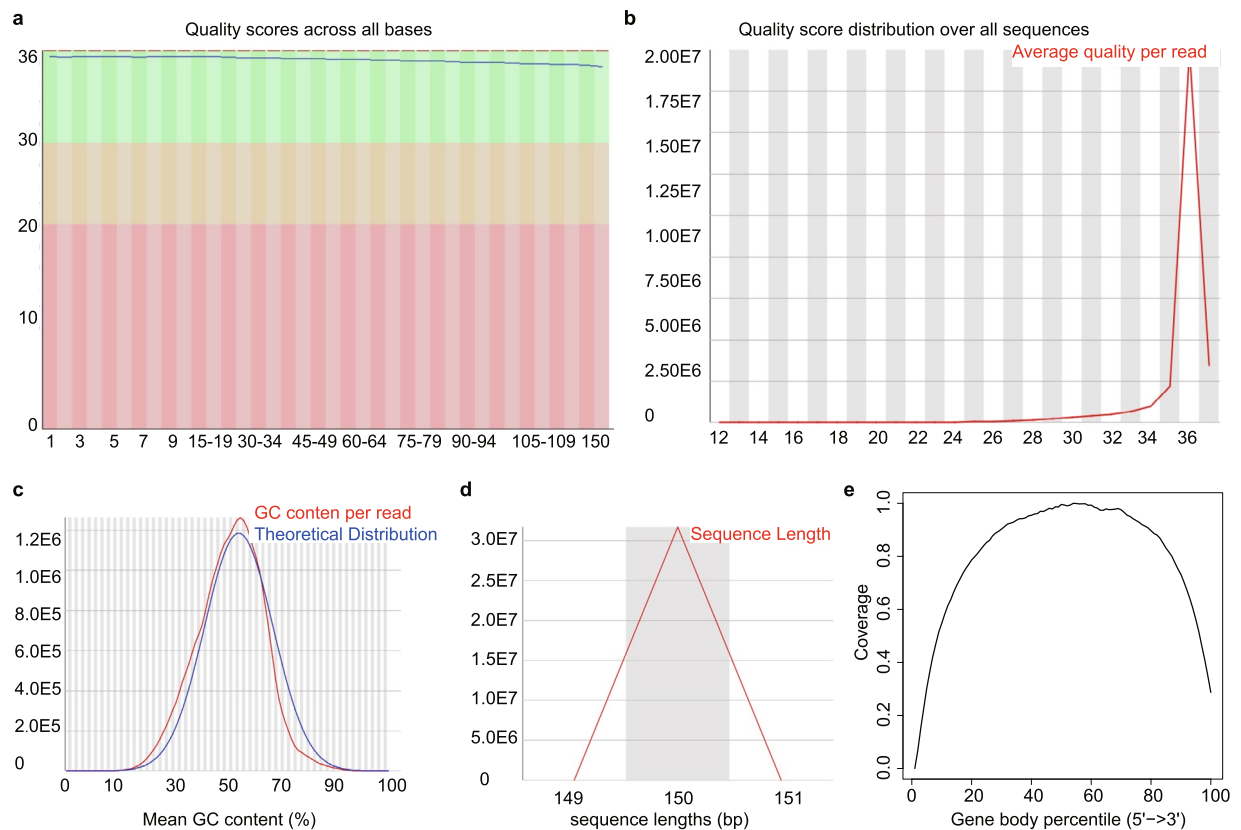


Fig. 3 Representative quality check of RNA-seq. **(a)** Representative quality score distribution for all 150 bp bases. **(b)** Representative quality score distribution of all sequences. **(c)** Representative distribution of GC content for each sequence. **(d)** Representative distribution of sequence length. **(e)** Coverage uniformity along with transcripts.

SVF (Fig. 2b). The above results suggested that SVF cells in the control groups differentiate into the right subtype of adipocytes and that EGCG inhibits SVF cell adipogenic differentiation.

Quality control of RNA integrity. The quality of total RNA was examined by an Agilent Bioanalyzer 2100. All of the samples showed high RNA integrity (RIN value ranging from 7.7 to 10) and could be used for downstream sequencing.

RNA-Seq data quality. The raw RNA-seq data quality was determined by FastQC. A representative FastQC report is depicted in Fig. 3. As indicated, the reads had universally high-quality values (Fig. 3a,b). The distribution of GC content was similar to the theoretical distribution, which indicates that the samples were free from contamination (Fig. 3c). Meanwhile, the sequence length distribution showed a peak only at 150 bp, which corresponded to the fragment sizes of the RNA-seq libraries (Fig. 3d). Then, the geneBodyCoverage.py script from the RseqQC package was used to assess the quality of the reads and no significant 5' or 3' end bias was identified (Fig. 3e). In addition, all other fastqc files showed similar reports and were qualified for downstream analysis. Subsequently, a very high percentage (more than 87.57%) of reads were mapped to the reference genome mm9 (Table 2). Next, the genes expression levels were examined. The box plot showed that the global expression levels of mRNA in all samples were similar (Fig. 4a). Furthermore, analysis of all the expressed genes by PCA plot showed that samples derived from a different tissue, time points, and treatment fell into distinct groups, suggesting variability between groups. Meanwhile, the biological replicates settled near each other, indicating high repeatability (Fig. 4b).

Identification of genes affected by EGCG. To identify the genes affected by EGCG, gene expression levels of the control and EGCG-treated groups were analyzed by DESeq2. The threshold criteria were set as $p\text{-adj} < 0.01$ and absolute $(\log_2 \text{FoldChange}) > 1$. The genes that met these criteria were further analyzed with a heatmap and volcano map. Figure 4c shows that the samples from the control groups and the EGCG-treated groups fell into two separate groups, indicating that EGCG robustly affects gene expression during adipogenesis. In addition, samples from triplicate replication were densely clustered, indicating high repeatability. Figure 4d shows that the EGCG regulated the expression of many genes, and the top significantly differentially expressed genes ordered by $p\text{-adj}$ were *Cep170b*, *Pdpm*, *Soc1*, *Slc39a6*, and *Pidd1*.

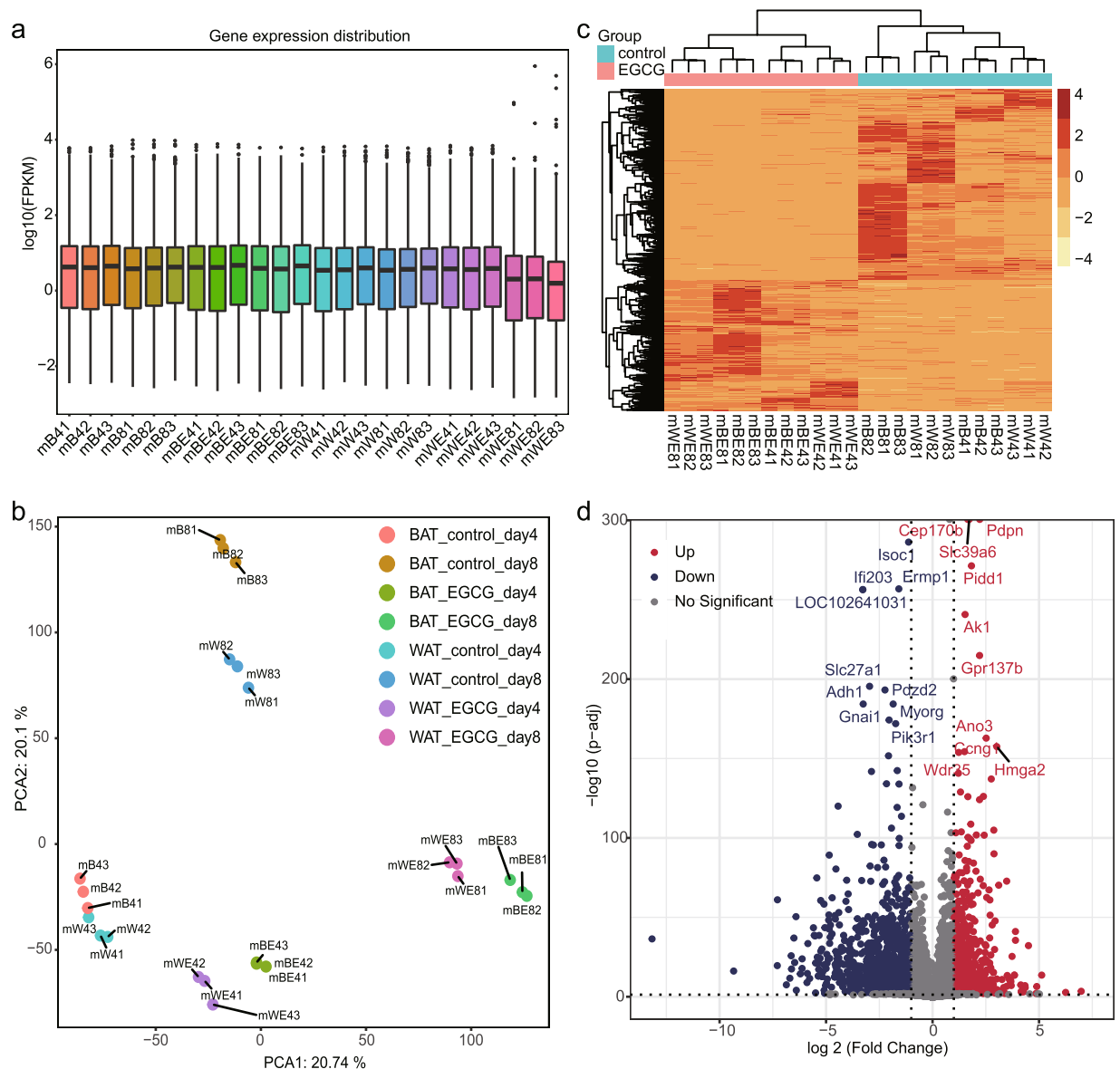


Fig. 4 (a) Box plot showing the expression level of mRNA in all samples. (b) Principal component analysis results. (c) Heatmap showing differentially expressed genes between EGCG treated and control cells. (d) Volcano plot comparing gene expression levels between EGCG treated and control cells. Red indicates significantly upregulated genes, while blue indicates significantly downregulated genes. The names of the top 20 significantly regulated genes arranged by p-adj are labeled.

Usage Notes

RNA-seq has been widely used to study gene expression in recent decades. It is a powerful method to systematically determine the molecular pathways affected by bioactive substances. Recently, EGCG has been recognized as one of the natural products with high anti-obesity efficacy. The data could provide important findings of the genes regulated by EGCG in adipogenesis and provide information about the role of EGCG in lipid accumulation and fat metabolism.

One major advantage of the data is that detailed stage- and tissue-specific gene expression profiles affected by EGCG were investigated. The data may be valuable to obesity-related clinical/basic research. Of note, RNA from the three replications was collected simultaneously, but the third replication was not sequenced at the same time as the other two. Although the quality of all RNA met the requirements of RNA-seq, it would be beneficial to correct the batch effect.

Code availability

In the current study, the following open access software was used as described in the Methods section. For all the software, we used default parameters, and no custom code was used beyond the tools listed.

1. FastQC (version 0.11.9) was used to check the quality of raw FASTQ sequencing data: <http://www.bioinformatics.babraham.ac.uk/projects/fastqc/>.
2. Fastp (version 0.20.1) was used to trim adapters and filter quality reads: <https://github.com/OpenGene/fastp>.
3. HISAT2 (version 2.2.0) was used to map sequence reads to the mouse mm9 genome: <http://daehwankimlab.github.io/hisat2/>.
4. DESeq2 (version 1.10.1) was used to identify differentially expressed genes: <https://bioconductor.org/packages/release/bioc/html/DESeq2.html>.
5. FactoMineR (version 2.4) was used to perform PCA: <https://cran.r-project.org/web/packages/FactoMineR/index.html>.
6. Pheatmap (Version 1.0.12) was used to plot the heatmap: <https://cran.r-project.org/web/packages/pheatmap/>.
7. Ggplot2 (version 3.3.4) was used to generate the volcano plot: <https://cran.r-project.org/web/packages/ggplot2/index.html>.
8. The Combat_Seq function from R package SVA was used to correct the batch effect of samples in each batch: <https://bioconductor.org/packages/release/bioc/html/sva.html>.
9. The GeneBodyCoverage.py script from RseqQC package (version 4.0.0) was used to evaluate the quality of the reads: <https://sourceforge.net/projects/rseqqc/files/>.

Received: 5 July 2021; Accepted: 23 December 2021;

Published online: 08 February 2022

References

1. Blüher, M. Obesity: global epidemiology and pathogenesis. *Nat. Rev. Endocrinol.* **15**, 288–298, <https://doi.org/10.1038/s41574-019-0176-8> (2019).
2. Stefan, N. Causes, consequences, and treatment of metabolically unhealthy fat distribution. *Lancet Diabetes Endocrinol* **8**, 616–627, [https://doi.org/10.1016/S2213-8587\(20\)30110-8](https://doi.org/10.1016/S2213-8587(20)30110-8). (2020).
3. Ikeda, K., Maretich, P. & Kajimura, S. The Common and Distinct Features of Brown and Beige Adipocytes. *Trends Endocrinol. Metab.* **29**, 191–200, <https://doi.org/10.1016/j.tem.2018.01.001> (2018).
4. Maurer, S., Harms, M. & Boucher, J. The colorful versatility of adipocytes: white-to-brown transdifferentiation and its therapeutic potential in humans. *FEBS J* (2020).
5. Ammori, B. *et al.* Medical and surgical management of obesity and diabetes: what's new? *Diabet. Med.* **37**, 203–210 (2020).
6. Martel, J. *et al.* Anti-obesogenic and antidiabetic effects of plants and mushrooms. *Nat. Rev. Endocrinol* **13**, 149 (2016).
7. Cavet, M. E., Harrington, K. L., Vollmer, T. R., Ward, K. W. & Zhang, J.-Z. Anti-inflammatory and anti-oxidative effects of the green tea polyphenol epigallocatechin gallate in human corneal epithelial cells. *Mol. Vis.* **17**, 533 (2011).
8. Gao, Z. *et al.* Targeting HO-1 by epigallocatechin-3-gallate reduces contrast-induced renal injury via anti-oxidative stress and anti-inflammation pathways. *PLoS ONE* **11**, e0149032 (2016).
9. Wang, J., Man, G. C. W., Chan, T. H., Kwong, J. & Wang, C. C. A prodrug of green tea polyphenol (–)-epigallocatechin-3-gallate (Pro-EGCG) serves as a novel angiogenesis inhibitor in endometrial cancer. *Cancer Lett.* **412**, 10–20 (2018).
10. Wolfram, S. Effects of green tea and EGCG on cardiovascular and metabolic health. *J. Am. Coll. Nutr.* **26**, 373S–388S (2007).
11. Li, F. *et al.* EGCG Reduces Obesity and White Adipose Tissue Gain Partly Through AMPK Activation in Mice. *Front Pharmacol* **9**, 1366–1366, <https://doi.org/10.3389/fphar.2018.01366> (2018).
12. Lee, M. S., Shin, Y., Jung, S. & Kim, Y. Effects of epigallocatechin-3-gallate on thermogenesis and mitochondrial biogenesis in brown adipose tissues of diet-induced obese mice. *Food Nutr Res* **61**, 1325307, <https://doi.org/10.1080/16546628.2017.1325307> (2017).
13. Zhang, P.-p. *et al.* Identification of Circular RNA Expression Profiles in White Adipocytes and Their Roles in Adipogenesis. *Front Physiol* **12**, <https://doi.org/10.3389/fphys.2021.728208> (2021).
14. Zhang, P. *et al.* Assessment of CircRNA Expression Profiles and Potential Functions in Brown Adipogenesis. *Front Genet* **12**, <https://doi.org/10.3389/fgene.2021.769690> (2021).
15. Shan, T. *et al.* Adipocyte-specific deletion of mTOR inhibits adipose tissue development and causes insulin resistance in mice. *Diabetologia* **59**, 1995–2004, <https://doi.org/10.1007/s00125-016-4006-4> (2016).
16. FastQC. FastQC: a quality control tool for high throughput sequence data. (2016).
17. Chen, S., Zhou, Y., Chen, Y. & Gu, J. fastp: an ultra-fast all-in-one FASTQ preprocessor. *Bioinformatics (Oxford, England)* **34**, i884–i890, <https://doi.org/10.1093/bioinformatics/bty560> (2018).
18. Kim, D., Paggi, J. M., Park, C., Bennett, C. & Salzberg, S. L. Graph-based genome alignment and genotyping with HISAT2 and HISAT-genotype. *Nat. Biotechnol.* **37**, 907–915 (2019).
19. Anders, S., Pyl, P. T. & Huber, W. HTSeq—a Python framework to work with high-throughput sequencing data. *Bioinformatics* **31**, 166–169 (2015).
20. Zhang, Y., Parmigiani, G. & Johnson, W. E. ComBat-seq: batch effect adjustment for RNA-seq count data. *NAR Genom Bioinform* **2**, lqaa078 (2020).
21. Lê, S., Josse, J. & Husson, F. FactoMineR: an R package for multivariate analysis. *J Stat Softw* **25**, 1–18 (2008).
22. Kolde, R. & Kolde, M. R. Package ‘pheatmap’. *R package* **1**, 790 (2015).
23. Wickham, H. ggplot2. *Wiley Interdiscip Rev Comput Stat* **3**, 180–185 (2011).
24. Zhang, P., Xu, Y., Xu, H. & Li, C. RNA-seq to determine the effect of EGCG on gene expression during WAT and BAT preadipocyte differentiation. *NCBI Sequence Read Archive* <http://identifiers.org/ncbi/insdc.sra:SRP318155> (2021).

Acknowledgements

We thank our lab members for their discussion and comments. This work was financially supported by the National Natural Science Foundation of China (31601167, 31972537), the Major Science and Technology Projects of Henan Province (201300111200), the Department of Education in Henan Province (21A230017), and the Nanhu Scholars Program of XYNU.

Author contributions

P.Z. conceived the project and designed the experiments, P.Z., Y.X., C.L. and H.X. analyzed the data and wrote the manuscript. P.Z., W.W., X.J., Y.W., Q.H. and C.D. performed the experiments.

Competing interests

The authors declare no competing interests.

Additional information

Correspondence and requests for materials should be addressed to C.L. or Y.X.

Reprints and permissions information is available at www.nature.com/reprints.

Publisher's note Springer Nature remains neutral with regard to jurisdictional claims in published maps and institutional affiliations.



Open Access This article is licensed under a Creative Commons Attribution 4.0 International License, which permits use, sharing, adaptation, distribution and reproduction in any medium or format, as long as you give appropriate credit to the original author(s) and the source, provide a link to the Creative Commons license, and indicate if changes were made. The images or other third party material in this article are included in the article's Creative Commons license, unless indicated otherwise in a credit line to the material. If material is not included in the article's Creative Commons license and your intended use is not permitted by statutory regulation or exceeds the permitted use, you will need to obtain permission directly from the copyright holder. To view a copy of this license, visit <http://creativecommons.org/licenses/by/4.0/>.

The Creative Commons Public Domain Dedication waiver <http://creativecommons.org/publicdomain/zero/1.0/> applies to the metadata files associated with this article.

© The Author(s) 2022